Electronic Structure and Charge-Transport Properties of N,N′-Bis(cyclohexyl)naphthalene Diimide

ARTICLE *in* THE JOURNAL OF PHYSICAL CHEMISTRY C · JANUARY 2010

Impact Factor: 4.77 · DOI: 10.1021/jp9096937

2 AUTHORS, INCLUDING:

Shashishekar P Adiga
Lockheed Martin Corporation
26 PUBLICATIONS **411** CITATIONS

Electronic Structure and Charge-Transport Properties of *N*,*N*′-Bis(cyclohexyl)naphthalene Diimide

Shashishekar P. Adiga* and Deepak Shukla

Kodak Research Laboratories, Eastman Kodak Company, Rochester, New York 14650

Received: October 9, 2009; Revised Manuscript Received: December 10, 2009

The charge-transport properties of *N*,*N*′-bis(cyclohexyl)naphthalene diimide (NDI-CHEX) crystals are explored via quantum chemical calculations. Electronic coupling elements in different dimer configurations taken from the crystal are calculated by use of density functional theory. Electron transport bandwidths are derived from one-dimensional molecular stacks along key crystallographic directions. The results indicate that charge transport is confined to (001) planes, which are also the preferred thin-film deposition planes. The calculations also reveal that the most preferred pathway for electron transport is the family of ⟨110⟩ directions.

1. Introduction

There has been active research into finding a suitable n-channel organic semiconductor material.[1] The most extensive work thus far on n-type molecular organic semiconductors has involved naphthalene diimide (NDI) and perylene diimide (PDI) based systems.[2−4] The applicability of these materials in optoelectronic devices such as organic thin-film transistors (TFT) is primarily determined by their ability to form well-defined molecular crystals. Specifically, whether these compounds allow for the preparation of well-ordered crystalline thin films is one of the key design considerations. Recently it was demonstrated that, by attaching cyclohexyl end groups to NDI, an efficient molecular stacking and thin-film morphology that leads to superior field effect mobility can be obtained.[5] Particularly, in TFTs made from NDI-CHEX, carrier mobility for electron transport up to 6 $cm^2/(V \cdot s)$ was observed. This high mobility was ascribed, on the basis of X-ray diffraction data, to the fact that the thin film of NDI-CHEX displayed a high order with a preferred crystallographic orientation in which (001) crystallographic planes lie parallel to the substrate. It is well-known that charge transport in many organic crystals is highly anisotropic and certain crystallographic planes and directions exhibit very high mobilities. In this context, it is important to correlate the transport behavior with the chemical structure and packing in the molecular crystal and examine whether the thin-film deposition plane corresponds to the preferred plane for charge transport.

A key issue in understanding charge transport in organic materials is to characterize the structural factors important to the conduction of electrons and holes. At the microscopic level, two limiting mechanisms of charge transport have been observed.[6,7] In single crystals at low temperature, a band regime akin to conventional inorganic semiconductors can occur. In this regime, charge transport takes place in delocalized states and is limited by the scattering of the carriers due to phonons, and thus the mobility decreases with temperature. At higher temperatures and in the presence of structural disorders, however, the band model becomes invalid in many organic semiconductors, as the mean free path of carriers becomes smaller than the distance between two adjacent molecules. This leads to a high-temperature regime where the charge carriers get localized over single molecule and transport behavior is governed by a thermally activated hopping mechanism.[8] This hopping mechanism is described as an electron (hole) transfer from a charged monomer to an adjacent neutral monomer. The rate at which charge transfer occurs in this self-exchange reaction, in the context of semiclassical Marcus electron-transfer theory,[9,10] may be written as

$$W = \frac{t^2}{\hbar}\left(\frac{\pi}{\lambda k_B T}\right)^{1/2} \exp\left(-\frac{\lambda}{4k_B T}\right) \quad (1)$$

where k_B is the Boltzmann constant and T is the temperature. The rate is primarily determined by two molecular parameters: (i) transfer integral t, the electronic coupling between adjacent molecules, and (ii) the reorganization energy λ. Whether transport occurs by a bandlike or hopping mechanism, the crystal packing of the molecules plays an important role in determining the mobility of organic semiconductors. In this regard, electronic structure and bandwidth calculations have proven extremely useful in understanding the structure−property correlations in organic electronic materials.[11]

In the present work, we use quantum chemical calculations to elucidate the electronic structure of NDI-CHEX. The electronic structure and charge-transport characteristics were investigated by the density functional theory (DFT) method. First, a molecular quantum chemical approach is used to study the electronic structure of an individual molecule. Then we determine the charge-transfer integrals for different transfer pathways in the NDI-CHEX crystal by considering pairwise intermolecular interactions in various crystallographic directions. We also estimate the reorganization energy associated with charge transfer in an isolated NDI-CHEX molecule.

2. Theoretical Method

Unless otherwise stated, all monomer and dimer calculations were performed with DFT using the Gaussian03 package[12] with the B3LYP hybrid functional[13,14] and a 6-31G** basis set. Gas-phase geometry optimizations on isolated neutral and charged molecules were performed at this level. All open-shell calculations (radical ions) were

* To whom correspondence should be addressed: e-mail s.p.adiga@kodak.com.

10.1021/jp9096937
Published on Web 01/27/2010

performed with the unrestricted method (UB3LYP). Optimized neutral monomer geometries were compared to those obtained experimentally via X-ray diffraction. The calculated gas-phase energy gap separating the highest occupied molecular orbital (HOMO) and lowest unoccupied molecular orbital (LUMO) states is 3.61 eV. In comparison, the experimental optical band-gap value in hexane determined from absorption spectra is 3.26 eV. A time-dependent density functional theory (TDDFT) calculation on the B3LYP/6-31G**-optimized neutral molecule yielded a corrected gap of 3.21 eV, which matches well with the experimental gap value.

The reorganization energy λ is defined as the sum of geometrical relaxation energies of the two molecules involved in the hopping process. Here, we consider only the intramolecular contribution to the reorganization energy and neglect the contribution from the surroundings. The intramolecular reorganization energy (λ) associated with an intermolecular electron-transfer reaction consists of two terms related to the geometry relaxation energies upon going from the neutral state to a charged molecular state and vice versa; it is given by[15,16]

$$\lambda = (E^*_{ion} - E_{ion}) + (E^* - E) \quad (2)$$

For an electron (hole) hopping process, E and E^* are the optimized ground-state energy of the neutral molecule and the energy of the neutral molecule in the anionic (cationic) geometry, respectively; E_{ion} is the optimized energy of the anion (cation), and E^*_{ion} is the energy of the anion (cation) at the optimal geometry of the neutral molecule. The reorganization energy for NDI-CHEX was calculated by two methods. In method 1, the energy was computed directly from the adiabatic potential-energy surfaces of neutral/cation and neutral/anion species by use of eq 2.[15,16] In method 2, it was obtained on the basis of a normal-mode analysis, which provides partition of the total reorganization energy into contributions from each vibrational mode.[11,17,18] The normal-mode analyses of isolated NDI-CHEX molecules were performed with the DUSHIN code.[18] Quantum-mechanical geometry optimizations and frequency calculations were performed at the DFT-B3LYP level using the 6-31G** basis set.

For calculating the transfer integral, t, between two adjacent molecules, we use the Marcus−Hush[9,10,19] two-state model wherein two states, the HOMO and the LUMO, are assumed for each monomer. Due to electrostatic interactions between the monomers, degeneracy of the monomer levels splits, giving rise to four levels for the neutral dimer, which correspond to the HOMO − 1, HOMO, LUMO, and LUMO + 1 levels. The transfer matrix elements for the hole and electron conductors in a homomolecular system with same site energies are calculated as

$$t_e = \frac{1}{2}(E_{LUMO+1} - E_{LUMO}) \quad (3)$$

for electrons and

$$t_h = \frac{1}{2}(E_{HOMO} - E_{HOMO-1}) \quad (4)$$

for holes.

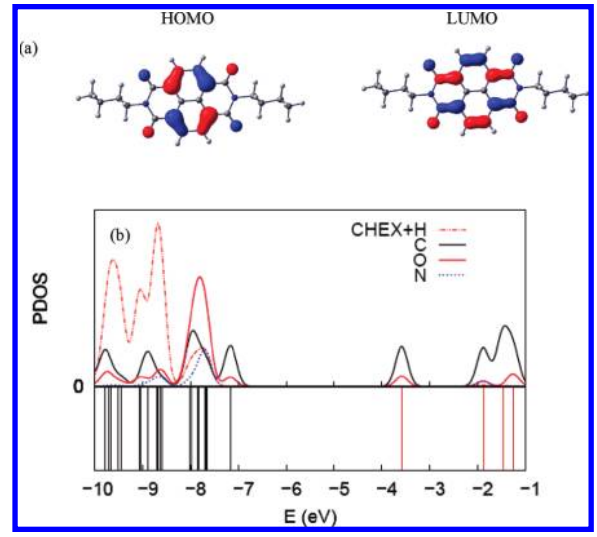

Figure 1. (a) B3LYP/6-31G** wave functions of the frontier molecular orbitals in isolated NDI-CHEX molecule. (b) MO energy levels (bottom) and PDOS for different groups of atoms (top) in the energy window between −10 and −1 eV. The energy levels are colored black and red for occupied and virtual orbitals, respectively.

The calculations of transfer matrix elements were performed at the following levels of theory: the semiempirical ZINDO/S (Zerner's implementation of intermediate neglect of differential overlap) Hamiltonian[20,21] and the DFT/B3LYP/6-31G** quantum mechanical calculations.

In addition to the dimer splitting, we analyzed the evolution of the bandwidth using the ZINDO method. In the framework of tight-binding theory, the bandwidth of a one-dimensional molecular stack is equal to $4t \cos[\pi/(N+1)]$, where t is the intermolecular transfer integral and N is the number of molecular units in the stack.[22] On the basis of the single-crystal structure of NDI-CHEX[23] a stack of N monomers in a given crystallographic direction was considered for these calculations.

3. Results

3.1. Molecular Electronic Structure. The B3LYP/6-31G** optimized and the X-ray diffraction (XRD) derived geometries of the neutral NDI-CHEX molecule are shown together in Figure S1of the Supporting Information. The wave functions for HOMO and LUMO are shown in Figure 1a. In Figure 1b, the molecular orbital energy levels and the partial density of states (PDOS) for different groups of atoms in the energy window between −10 and −1 eV are plotted. The total DOS is separated into contributions from O, N, C atoms belonging to NDI and all the remaining atoms. The dominant contributing orbitals to HOMO and LUMO are the p_z orbitals of C atoms. There is a notable contribution to HOMO and LUMO from O atoms as well. The majority of the molecular orbital density in the HOMO and LUMO orbitals resides on C atoms and is delocalized along the C−C bonds. While the LUMO is delocalized on C−C bonds parallel to the molecular axis, the HOMO is delocalized on C−C bonds that lie at an angle to the long axis. Because the π-orbital wave functions form nodes at the two nitrogen positions in the diimide rings, the cyclohexyl groups do not contribute to the frontier orbitals and are important only to attain the desired thin-film structure.

The hole and electron injection energies provide useful information regarding the organic TFT performance characteristics and its ambient stability. We have obtained the vertical ($E^*_{ion} - E$, difference between the radical ion and the neutral

TABLE 1: Electronic Properties of NDI-CHEX[a]

	E_{ie} (eV)		E_{ih} (eV)	
HOMO−LUMO GAP (eV)	vertical	adiabatic	vertical	adiabatic
3.61	−1.87	−2.05	8.43	8.32

[a] Properties listed are the B3LYP/6-31G**-calculated HOMO−LUMO gap and adiabatic and vertical injection energies for electrons (E_{ie}) and holes (E_{ih}).

TABLE 2: Calculated Intramolecular Reorganization Energies for Hole (λ^h) and Electron (λ^e) Transfer

λ^e (meV)		λ^h (meV)	
method 1	method 2	method 1	method 2
360	362	202	221

energies both calculated at the ground-state neutral geometry) and adiabatic ionization potentials (IPs) ($E_{ion} - E$, total energy difference between the fully relaxed radical ion and the ground-state neutral molecule). The HOMO−LUMO gap and ionization potentials for NDI-CHEX are presented in Table 1. The electron affinity is given by E_{ie}, the energy to inject an electron. Negative values of E_{ie} indicate exothermicity of the reduction of a molecule. The vertical injection energies for holes (E_{ih}) and electrons (E_{ie}) obtained in this work are very similar to the calculated values of 7.28 and −2.19 eV, respectively, for methyl-PDI.[24] The small difference in vertical and adiabatic values indicates that the structural relaxation upon charge injection is small.

3.2. Reorganization Energy. Internal reorganization energies for hole and electron transfers as calculated from adiabatic potential surface (method 1) and normal-mode analysis (method 2) are listed in Table 2. Results from the two methods show reasonable agreement. The reorganization energy for electrons is about 80% higher than that for holes. The significantly higher reorganization energy is supported by a larger relaxation with respect to the neutral geometry in the case of radical anion as compared to the radical cation (Figure S2, Supporting Information).

To further analyze the origin of the reorganization energy, the anionic and cationic reorganization energies were decomposed into contributions from individual normal modes.[18] Partition of the reorganization energy into the contributions of each normal mode is given in the Supporting Information in Tables S1 and S2 for anion and cation, respectively. The main contributions to the reorganization energy for the anion originate in vibrational modes in the range 1400−1720 cm^{-1}. The vibrational modes yielding the largest contribution to the reorganization energies for the anion are at 1404, 1650, and 1718 cm^{-1}. These three modes, confined to the NDI core, are depicted in Figure 2. It is noted that the naphthalene core contributes most to the modes 1404 and 1650 cm^{-1} and symmetric carbonyl stretching is responsible for the 1718 cm^{-1} mode. In comparison, the reorganization energies of pentyl-attached PDI (PDI-C5), a closely related n-channel material, for electron and hole transfer have been calculated to be 272 and 163 meV, respectively.[3] The lower reorganization energies for PDI-C5 are explained on the basis of a larger number of C atoms (24) in the PDI-C5 core and, hence, a greater extent of delocalization of frontier orbitals as compared to the NDI-CHEX core, which has only 14 C atoms.

3.3. Transfer Integrals and Band Evolution along Crystallographic Directions. The unit cell of NDI-CHEX crystal (Figure 3) is defined by $a = 8.5410$ Å, $b = 6.6780$ Å, $c = 18.4270$ Å, and $\beta = 102.48°$.[23] The crystal structure leads to

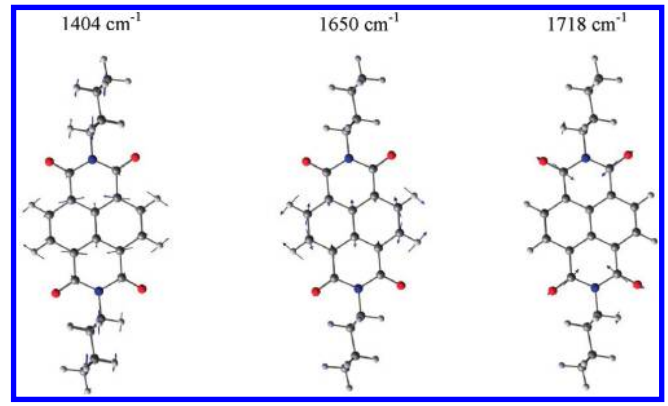

Figure 2. Normal modes that contribute the most to the anionic relaxation energy.

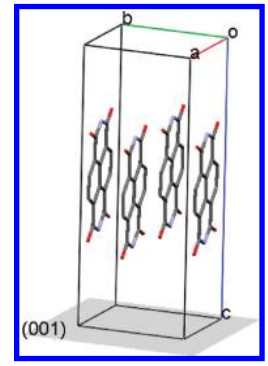

Figure 3. Unit cell of NDI-CHEX. The thin-film stacking plane (001) plane is marked. Hydrogen atoms and cyclohexyl groups are not shown for clarity.

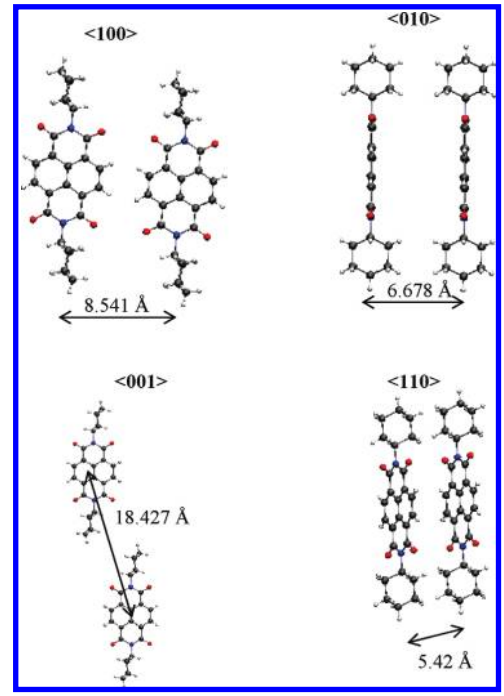

Figure 4. Unique neighbor arrangements: dimer types considered in our calculations of transfer integrals.

four types of dimers, which are nearest neighbors along the ⟨100⟩, ⟨010⟩, ⟨001⟩, and ⟨110⟩ directions. Figure 4 shows these four dimers along with the intermolecular distances. Other dimer possibilities were ignored due to longer intermolecular distances, such that any electronic coupling is not anticipated. The atomic coordinates as determined by X-ray diffraction on the single

TABLE 3: Effective Transfer Integrals[a]

	t_e		t_h	
dimer	B3LYP	ZINDO	B3LYP	ZINDO
⟨100⟩	18.91	3.54	1.36	0.54
⟨010⟩	0	0.3	0.0	0.3
⟨001⟩	0	0	0	0
⟨110⟩	91.43	78.50	79.59	125.86

[a] t_e and t_h are the effective transfer integrals for electrons and holes, respectively, calculated for NDI-CHEX dimers with the DFT/B3LYP/6-31G** and ZINDO methods.

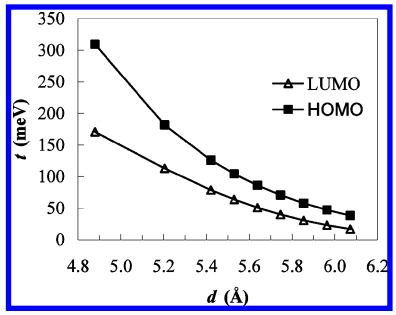

Figure 5. Evolution of the ZINDO-calculated HOMO and LUMO transfer integrals in a ⟨110⟩ dimer as a function of the intramolecular distance.

crystal[23] were used in dimer calculations without further geometry optimization.

The transfer integrals of these four nearest-neighbor dimers as calculated from DFT/B3LYP/6-31G** and ZINDO methods are listed in Table 3. The results from the two methods agree reasonably well. The largest electronic couplings are derived for dimers along the diagonal ⟨110⟩ direction. The ⟨110⟩ dimers have the shortest intermolecular spacing of all the dimers and are essentially in a displaced cofacial configuration. While the intermolecular distance is 5.42 Å, the overlapping regions of the naphthalene cores of the two molecules are just ca. 3.4 Å apart. In comparison, the ⟨100⟩ dimers are in an edge-on-edge conformation and have the shortest C to C spacing of 3.73 Å. The calculations reveal the absence of any electronic coupling in ⟨001⟩ and ⟨010⟩ dimers. The absence of electronic coupling along ⟨001⟩ suggests that charge transport is confined to the (001) plane.

The value of transfer integral depends on the intermolecular distance (d), and a small difference in this distance may lead to considerable change in charge-transport properties.[25] To analyze the dependence of t on d, calculations of frontier orbital splittings with incrementally varied distance between the centers of mass between the two molecules, in the range 4.8 Å < d < 6.2 Å, were also performed. In Figure 5, the variation of ZINDO-calculated t as a function of d is given for the ⟨110⟩ dimer. The value of t was found to decrease exponentially with respect to the distance between the two molecules. An interesting observation is that the transfer integral decreases by as much as 19% between d = 5.4 and 5.5 Å, which amounts to a decrease in charge-transfer rate (from eq 1) by ca. 34%. Thus an increase in lattice constant of as little as 0.1 Å can lead to a drastic change in charge-transport properties.

We now discuss the evolution of the total HOMO and LUMO bandwidths formed by the interaction of molecules in a one-dimensional stack along different crystallographic directions. The widths of the HOMO and LUMO bands, calculated at the ZINDO level, are plotted in Figure 6 as a function of cos [$\pi/(N + 1)$], where N is the number of NDI-

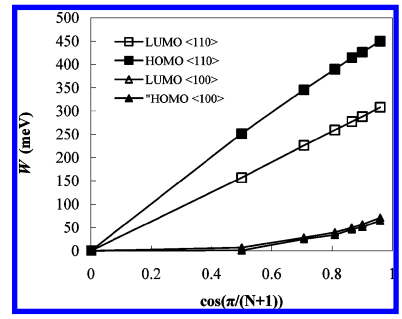

Figure 6. Evolution of ZINDO-calculated bandwidths (W) formed by the HOMO and LUMO levels of NDI-CHEX along ⟨110⟩ and ⟨100⟩ directions as a function of cos [$\pi/(N + 1)$], with N being the number of interacting molecules.

CHEX molecules in the one-dimensional array. Significant transfer integrals are found only along ⟨110⟩ directions and lead to HOMO and LUMO bandwidth values of 478 and 322 meV. The HOMO and LUMO bandwidths along the ⟨100⟩ direction were calculated to be 76 and 81 meV, respectively. It is useful to compare the bandwidth values for cofacial ⟨110⟩ dimers with those previously obtained for PDI-based crystals by the same approach.[1] In the case of PDI crystals, the ZINDO calculated bandwidths for dimers along the π-stacking directions are 545 and 225 meV for HOMO and LUMO, respectively. On the other hand, for molecular crystals of PDI-C5, HOMO and LUMO bandwidths were calculated to be 589 and 424 meV, respectively. Much of the difference in these bandwidth values can be attributed to differences in stacking between these crystals along the direction of interest. The intermolecular distance (distance between centers of mass of two molecules) and displacements along the short and long molecular axes between the cofacial dimer pairs are 5.421, 3.34, and 0 Å, respectively, for NDI-CHEX. The corresponding values are equal to 3.343, 1.31, and 3.11 Å in PDI-C5 and to 3.342, 1.10, and 3.37 Å in PDI, respectively.

4. Conclusions

To summarize, the key molecular parameters governing charge transport in the NDI-CHEX crystal have been determined by DFT calculation. Our investigation of crystal structure dimers predicts that the largest electronic coupling occurs in dimers along the ⟨110⟩ direction, followed by a significantly lower coupling for dimers along the ⟨100⟩ direction. On the basis of dimer transfer integral calculations and bandwidth calculations, it can be concluded that charge transfer is confined to the (001) plane, which is the experimentally observed thin-film device plane.[24] In addition, the most preferred pathway for electron transfer is along the ⟨110⟩ direction.

Supporting Information Available: Two figures and two tables as described in the text. This material is available free of charge via the Internet at http://pubs.acs.org.

References and Notes

(1) Newman, C. R.; Frisbie, C. D.; da Silva Filho, D. A.; Brédas, J. L.; Ewbank, P. C.; Mann, K. R. *Chem. Mater.* **2004**, *16*, 4436.

(2) Laquindanum, J. G.; Katz, H. E.; Dodabalapur, A.; Lovinger, A. J. *J. Am. Chem. Soc.* **1996**, *118*, 11331.

(3) Chesterfield, R. J.; McKeen, J. C.; Newman, C. R.; Ewbank, P. C.; da Silva Filho, D. A.; Brédas, J. L.; Miller, L. L.; Mann, K. R.; Frisbie, C. D. *J. Phys. Chem. B* **2004**, *108*, 1928.

(4) Katz, H. E.; Lovinger, A. J.; Johnson, J.; Kloc, C.; Siegrist, T.; Li, W.; Lin, Y.-Y.; Dodabalapur, A. *Nature* **2000**, *404*, 478.

(5) Shukla, D.; Nelson, S. F.; Freeman, D. C.; Rajeswaran, M.; Ahearn, W. G.; Meyer, D. M.; Carey, J. T. *Chem. Mater.* **2008**, *20*, 7486.
(6) Schein, L. B.; Duke, C. B.; McGhie, A. R. *Phys. Rev. Lett.* **1978**, *40*, 197.
(7) Schein, L. B.; Warta, W.; McGhie, A. R.; Karl, N. *Chem. Phys. Lett.* **1983**, *100*, 34.
(8) Horowitz, G. *Adv. Mater.* **1998**, *10*, 365.
(9) Marcus, R. A. *J. Chem. Phys.* **1956**, *24*, 966.
(10) Marcus, R. A. *Rev. Mod. Phys.* **1993**, *65*, 599.
(11) Coropceanu, V.; Cornil, J.; da Silva Filho, D. A.; Olivier, Y.; Silbey, R.; Bredas, J. L. *Chem. Rev.* **2007**, *107*, 926.
(12) Frisch, M. J.; Trucks, G. W.; Schlegel, H. B.; Scuseria, G. E.; Robb, M. A.; Cheeseman, J. R.; Montgomery, J. A., Jr.; Vreven, T.; Kudin, K. N.; Burant, J. C.; Millam, J. M.; Iyengar, S. S.; Tomasi, J.; Barone, V.; Mennucci, B.; Cossi, M.; Scalmani, G.; Rega, N.; Petersson, G. A.; Nakatsuji, H.; Hada, M.; Ehara, M.; Toyota, K.; Fukuda, R.; Hasegawa, J.; Ishida, M.; Nakajima, T.; Honda, Y.; Kitao, O.; Nakai, H.; Klene, M.; Li, X.; Knox, J. E.; Hratchian, H. P.; Cross, J. B.; Bakken, V.; Adamo, C.; Jaramillo, J.; Gomperts, R.; Stratmann, R. E.; Yazyev, O.; Austin, A. J.; Cammi, R.; Pomelli, C.; Ochterski, J. W.; Ayala, P. Y.; Morokuma, K.; Voth, G. A.; Salvador, P.; Dannenberg, J. J.; Zakrzewski, V. G.; Dapprich, S.; Daniels, A. D.; Strain, M. C.; Farkas, O.; Malick, D. K.; Rabuck, A. D.; Raghavachari, K.; Foresman, J. B.; Ortiz, J. V.; Cui, Q.; Baboul, A. G.; Clifford, S.; Cioslowski, J.; Stefanov, B. B.; Liu, G.; Liashenko, A.; Piskorz, P.; Komaromi, I.; Martin, R. L.; Fox, D. J.; Keith, T.; Al-Laham, M. A.; Peng, C. Y.; Nanayakkara, A.; Challacombe, M.; Gill, P. M. W.; Johnson, B.; Chen, W.; Wong, M. W.; Gonzalez, C.; Pople, J. A. *Gaussian 03, Revision C.02*; Gaussian, Inc.: Wallingford, CT, 2004.
(13) Becke, A. D. *J. Chem. Phys.* **1993**, *98*, 5648.
(14) Lee, C.; Yang, W.; Parr, R. G. *Phys. Rev. B* **1988**, *37*, 785.
(15) Malagoli, M.; Brédas, J. L. *Chem. Phys. Lett.* **2000**, *327*, 13.
(16) Deng, W. Q.; Goddard, W. A. *J. Phys. Chem. B* **2004**, *108*, 8614.
(17) Barbara, P. F.; Meyer, T. J.; Ratner, M. A. *J. Phys. Chem.* **1996**, *100*, 13148.
(18) Reimers, J. R. *J. Chem. Phys.* **2001**, *115*, 9103.
(19) Hush, N. S. *J. Chem. Phys.* **1958**, *28*, 962.
(20) Ridley, J.; Zerner, M. *Theor. Chem. Acta* **1973**, *32*, 111.
(21) Zerner, M. C.; Loew, G. H.; Kirchner, R. F.; Mueller-Westerhoff, U. T. *J. Am. Chem. Soc.* **1980**, *102*, 589.
(22) Cornil, J.; Beljonne, D.; Calbert, J. P.; Brédas, J. L. *Adv. Mater.* **2001**, *13*, 1053.
(23) Shukla, D.; Rajeswaran, M. *Acta Crystallogr.* **2008**, *E64*, o1735.
(24) Liang, B.; Zhang, Y.; Wang, Y.; Xu, W.; Li, X. *J. Mol. Struct.* **2009**, *917*, 133.
(25) Troisi, A.; Orlandi, G. *J. Phys. Chem. B* **2005**, *109*, 1849.

JP9096937